environments

MDPI

Article

Investigating the Cosmic and Solar Drivers of Stratospheric ^{7}Be Variability

Alessandro Rizzo [1,*], Giuseppe Antonacci [1], Massimo Astarita [1], Enrico Maria Borra [1], Luca Ciciani [1], Nadia di Marco [1], Giovanna la Notte [1], Patrizio Ripesi [2], Luciano Sperandio [1], Ignazio Vilardi [1] and Francesca Zazzaron [1]

[1] Institute of Radioprotection (IRP), C.R. Casaccia, ENEA—Italian National Agency for New Technologies, Energy and Sustainable Economic Development, Via Anguillarese 301, 00123 Rome, Italy; giuseppe.antonacci@enea.it (G.A.); massimo.astarita@enea.it (M.A.); enrico.borra@enea.it (E.M.B.); luca.ciciani@enea.it (L.C.); nadia.dimarco@enea.it (N.d.M.); giovanna.lanotte@enea.it (G.l.N.); luciano.sperandio@enea.it (L.S.); ignazio.vilardi@enea.it (I.V.); francesca.zazzaron@enea.it (F.Z.)

[2] ATM System Evolution and Strategic Services Planning, Enav S.p.a., Via Salaria 716, 00138 Rome, Italy; patrizio.ripesi@enav.it

* Correspondence: alessandro.rizzo@enea.it; Tel.: +39-06-30486206

Abstract

Space weather exerts a significant influence on the Earth's atmosphere, driving a variety of physical processes, including the production of cosmogenic radionuclides. Among these, ^{7}Be is a naturally occurring radionuclide formed through spallation reactions induced by cosmic-ray showers interacting with atmospheric constituents, primarily oxygen and nitrogen. Over long timescales, the atmospheric concentration of ^{7}Be exhibits a direct correlation with the cosmic-ray flux reaching the Earth and an inverse correlation with solar activity, which modulates this flux via variations of the heliosphere. The large availability of ^{7}Be concentration data, resulting from its use as a natural tracer employed in atmospheric transport studies and in monitoring the fallout from radiological incidents such as the Chernobyl disaster, can also be exploited to investigate the impact of space weather conditions on the terrestrial atmosphere and related geophysical processes. The present study analyzes a long-term dataset of monthly ^{7}Be activity concentrations in air samples collected at ground level since 1987 at the ENEA Casaccia Research Center in Rome, Italy. In particular, the linear correlation of this time series with the galactic cosmic ray flux on Earth and solar activity have been investigated. Data from a ground-based neutron monitor and sunspot numbers have been used as proxies for galactic cosmic rays and solar activity, respectively. A centered running-mean low-pass filter was applied to the monthly ^{7}Be time series to extract its low-frequency component associated with cosmic drivers, which is partially hidden by high-frequency modulations induced by atmospheric dynamics. For Solar Cycles 22, 23, 24, and partially 25, the analysis shows that a substantial portion of the relationship between stratospheric ^{7}Be concentrations and cosmic drivers is captured by linear correlation. Within a statistically consistent framework, the evidence supports a correlation between ^{7}Be and cosmic drivers consistent with solar-cycle variability. The ^{7}Be radionuclide can therefore be regarded as a reliable atmospheric tracer of cosmic-ray variability and, indirectly, of solar modulation.

Keywords: atmospheric ^{7}Be concentration; cosmic ray flux; solar activity; correlation; anti-correlation; cosmic drivers; solar drivers

Academic Editor: William A. Anderson

Received: 5 August 2025
Revised: 29 August 2025
Accepted: 1 September 2025
Published: 4 September 2025

Citation: Rizzo, A.; Antonacci, G.; Astarita, M.; Borra, E.M.; Ciciani, L.; di Marco, N.; la Notte, G.; Ripesi, P.; Sperandio, L.; Vilardi, I.; Zazzaro, F. Investigating the Cosmic and Solar Drivers of Stratospheric ^{7}Be Variability. *Environments* **2025**, *12*, 312. https://doi.org/10.3390/environments12090312

1. Introduction

Since the pioneering work of Libby [1], who hypothesized the production of radioactive isotopes in the development of atmospheric nuclear showers initiated by galactic cosmic rays, cosmogenic radionuclides have attracted growing scientific interest. Among them, ^{7}Be has been extensively investigated since its first detection in rainwater samples [2], due to its characteristic half-life, emission properties, and distinctive distribution across atmospheric layers. As a natural radioactive tracer, it is a key radionuclide for investigating physical phenomena ranging from atmospheric dynamics [3–6] to climate change [7,8], but also for monitoring the fallout of potential anthropogenic releases into the atmosphere, as in the case of the Chernobyl disaster in 1986 [9]. As a result, since 1987, environmental laboratories worldwide have started the systematic measurement of ^{7}Be concentrations in air (dry deposition) and rain (wet deposition) as part of their routine environmental monitoring programs [10]. Consequently, a vast amount of ^{7}Be concentration data has been accumulated over the years, providing valuable resources also for other areas of physics, such as planetary science and space weather research.

Cosmogenic ^{7}Be is present throughout the Earth's atmosphere with varying concentrations, with maxima occurring in both production and accumulation layers. Although stratospheric production (12–50 km) represents the predominant source of ^{7}Be detected at ground level due to its 53-day half-life, the isotope is also present at higher altitudes. Spectrometric measurements on the outer surfaces of spacecraft returning from low Earth orbit [11], as well as data from balloon-borne experiments [12,13], have indicated unexpectedly high ^{7}Be concentrations in the mesosphere (above 50 km) and lower thermosphere (above 85 km), suggesting the existence of additional production mechanisms in these regions.

In particular, SEPs (Solar Energetic Particles), whose lower energies compared to Galactic Cosmic Rays (GCRs) cause them to interact predominantly in the upper atmosphere, have been proposed as a possible source of additional ^{7}Be production. By generating particle showers at high altitudes, they may lead to localized modulation of ^{7}Be concentrations, as hypothesized for high-latitude regions [14].

Regarding the lower atmospheric layers, the dominant source of ^{7}Be remains associated to the interaction of higher-energy GCRs, which are able to penetrate into the stratosphere and trigger the spallation reactions responsible for its formation. This well-established mechanism explains the statistical dependence and correlation observed between GCR flux and stratospheric ^{7}Be concentrations. The GCR flux is modulated by the Sun, decreasing during periods of high solar activity because of the expansion of the heliosphere, which results from enhanced solar wind production and a stronger, more irregular interplanetary magnetic field. Scattering and diffusion processes of incoming GCRs within the expanded heliosphere lead to a reduction of their flux in the Solar System and on Earth [15,16]. As a consequence of this mechanism, there is a well-established anti-correlation between GCR flux and solar activity, which in turn translates into a direct anti-correlation between atmospheric ^{7}Be concentrations and solar activity.

In the environmental and atmospheric physics fields the correlation between the stratospheric ^{7}Be and solar activity at different time scale has been investigated by some authors [17–19] but only a few have also examined its correlation with the galactic cosmic ray flux on Earth at the same time [20].

This study focuses on the correlation between the monthly stratospheric ^{7}Be concentration, measured at the Casaccia Research Centre since 1987, and proxy variables of cosmic ray flux and solar activity, retrieved from open science databases. The use of long-term monthly time series provides an appropriate temporal framework for detecting relationships with cosmic drivers and characterizing multi-annual trends. A centered

running-mean low-pass filter has been applied to detrend the monthly ^{7}Be time series, to attenuate short-term atmospheric variability and to enable a clearer assessment of the signal component associated with cosmic drivers.

Phenomena such as the seasonal intrusion of stratospheric air into the troposphere (annual modulation) [21,22], the quasi-biennial oscillation (QBO) in stratospheric wind direction with a period of approximately 2.2 years [23], teleconnections with the El Niño–Southern Oscillation occurring on timescales of about 7 years [24], and semi-decadal oscillations [25] are all recognized contributors to ^{7}Be variability, and they can hide the low-frequency cosmic modulation signal. By disentangling these Earth-induced effects, this study aims to investigate whether the stratospheric ^{7}Be concentration can be considered as a proxy, or anti-proxy, for cosmic ray flux and solar activity.

2. Materials and Methods

2.1. Stratospheric ^{7}Be Production, Deposition and Measurement in Casaccia Research Center

The ^{7}Be isotope is produced in the Earth's atmosphere through interactions of galactic cosmic rays (GCR) predominantly with nitrogen and oxygen nuclei [26]. The production reactions are driven by spallation processes, mainly induced by protons and neutrons generated within the atmospheric shower initiated by a GCR. Examples of such reactions are given below:

$$p\,(n) + {}^{14}\mathrm{N} \rightarrow {}^{7}\mathrm{Be} + X \quad (1)$$

$$p\,(n) + {}^{16}\mathrm{O} \rightarrow {}^{7}\mathrm{Be} + Y \quad (2)$$

where X and Y denote the residual products of the respective spallation reactions. Considering the timescales of atmospheric diffusion processes (typically on the order of several weeks), the production of ^{7}Be can be assumed to occur quasi-simultaneously along the entire extent of the hadronic shower.

According to theoretical models (e.g., [27]), the ^{7}Be maximum production is reached in the stratosphere (10–50 km), where showers exhibit their maximum development [28]. Formed in ionized states as Be^{+} or Be^{2+}, beryllium rapidly attaches to sub-micron aerosol particles, whose high specific surface area enhances electrostatic interaction efficiency [29,30]. Once attached, ^{7}Be gradually drifts toward the ground due to gravitational settling and atmospheric dynamics, reaching deposition velocities of few cm s^{-1} [31]. The separation layer between the stratosphere and the troposphere, the tropopause (approximately at 12 km of altitude at considered latitudes), acts as an accumulation layer for ^{7}Be during its drifting. The strong reduction in vertical mixing, caused by the sharp gradient in temperature and density in this layer, effectively inhibits the downward transfer of air masses containing beryllium [32]. Approximately 71% of ^{7}Be is removed from the atmosphere by deposition processes, with about 68% of this fraction due to wet deposition (precipitation) and around 3% due to dry deposition (aerosol settling). The remaining 29% is lost through radioactive decay in the atmosphere [33,34]. Due to its characteristic single gamma emission at 477.6 keV, ^{7}Be is readily detectable on ground via gamma-ray spectrometry both in rainwater sample (wet deposition) and in aerosol samples collected on filters (dry deposition). In this study, only dry deposition data are available because the monitoring network in place at the Casaccia Research Center is designed for nuclear emergency preparedness, aiming to detect potential releases from the on-site nuclear facilities and the following plume passage. Air sampling is performed using three high-volume air samplers located within the site, each equipped with an eight-position filter carousel. Each filter is exposed for 24 h and the sampled air volume (≈800 $m^{3}day^{-1}$ per station) is measured by calibrated volumetric counters. At the end of each month, the 90 daily filters (3 stations for 30 days) are analyzed using low-background HPGe. The ENEA environmen-

tal laboratory is equipped with 8 HPGe co-axial detectors housed in Pb–Cu shielding to lowering the background, used to quantify the 477.6 keV line of ^{7}Be. Over its multi-decadal operation, the monitoring network has undergone periodic instrument renewals. To ensure long-term comparability, it operates under harmonized Quality Assurance and Quality Control (QA/QC) procedures agreed with the national competent authority, including traceable, geometry-matched calibrations, documented flow-meter checks with sampled-volume control, efficiency checks, and Minimum Detectable Activity (MDA) evaluation. These procedures ensure data quality, homogeneity and continuity of the ^{7}Be time series over the entire period of operation.

2.2. Datasets and Data Analysis

The upper panel (a) of Figure 1 shows the monthly time series of atmospheric ^{7}Be dry deposition, as measured at the Casaccia Research Center. The time series in the figure shows high-frequency contributions from atmospheric dynamics, superimposed on the 11-year solar-cycle contribution.

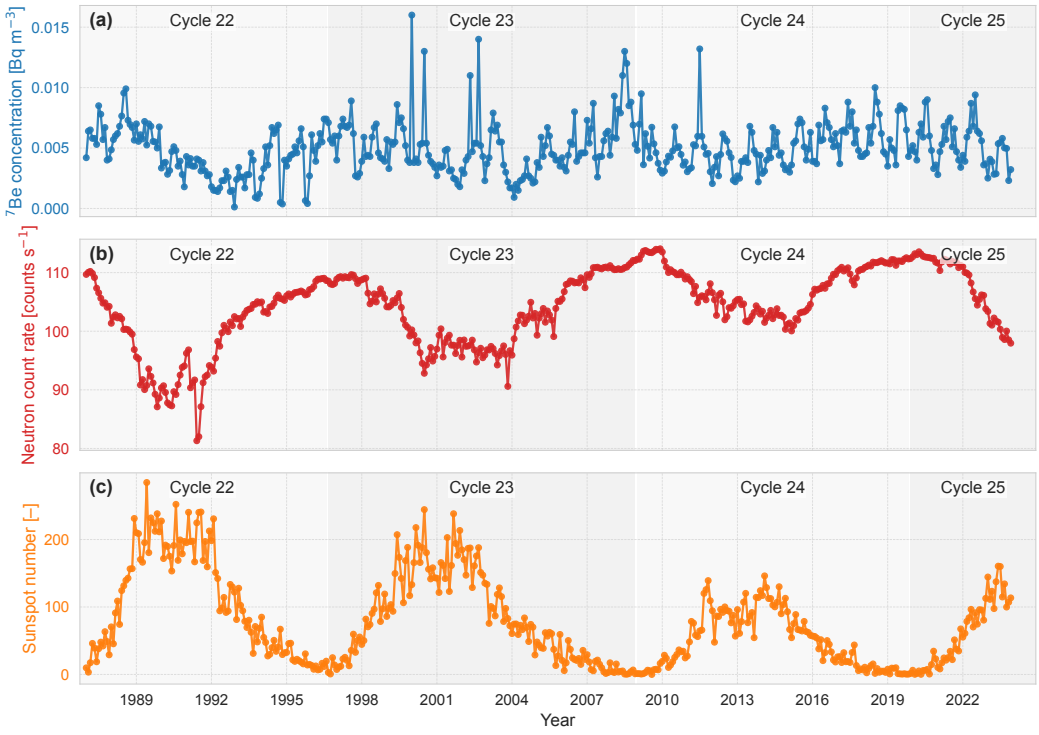

Figure 1. Monthly time series of atmospheric ^{7}Be concentrations at Casaccia (**a**), ground-level neutron monitor counts (**b**), and sunspot numbers (**c**) from 1987 to 2024. Neutron monitor data are taken as a proxy for galactic cosmic ray intensity, and sunspot numbers for solar activity. Shaded vertical bands denote solar cycles 22–25, with labels at the top of each panel.

The variables linked to the space weather conditions around our planet are available through two Open Science databases. In this work, neutron flux data from the Oulu station in Finland, part of the global neutron monitor network [35], are used as a proxy for GCR flux at Earth's surface. Neutrons, together with muons, are among the most penetrating particles produced in hadronic showers in the atmosphere and are capable of reaching the ground. For this reason, their flux is directly proportional to the incoming GCR flux impacting the Earth. Although Oulu is not the closest monitor to our sampling site, geomagnetic cut-off rigidity is not a discriminating factor for this analysis: for large-scale drivers such as GCR modulation the neutron signal is strongly coherent across stations, whereas the robustness of the results depends primarily on data quality (complete temporal coverage, continuity,

and outlier control). Oulu neutron monitor was therefore selected because it provides one of the longest, most continuous, and homogeneous European records, maximizing stability over the entire ^{7}Be time span.

The sunspot number data were retrieved from the Open Science database provided by [36]. The corresponding time series of cosmic and solar drivers are displayed in the middle (b) and bottom (c) panels of Figure 1.

2.3. Detrending of ^{7}Be Time Series

The presence of temporal modulations in the ^{7}Be time series, induced by atmospheric exchange processes with no counterparts in cosmic drivers, necessitates the application of detrending procedures to reliably quantify the correlation and the dependency between these variables. Their presence can indeed introduce artificial negative contributions in the covariance structure, potentially obscuring the true physical relationships under investigation.

Short-term variability in atmospheric ^{7}Be concentrations primarily reflects dynamic processes occurring in the troposphere and lower stratosphere, including seasonal cycles, quasi-biennial oscillations (QBO), stratosphere-troposphere exchange events, large-scale circulation patterns, and phenomena such as ENSO (El Niño–Southern Oscillation). These terrestrial drivers impart oscillations on timescales ranging from several months to a few years, superimposed upon longer-term variations controlled by solar activity and cosmic ray modulation. To achieve this separation of timescales a running average method with a fixed time window has been implemented as a low-pass filter. This classical approach, widely adopted in geophysical and climate sciences, is used to suppress high-frequency fluctuations and extract low-frequency trends [37,38].

In this work, the running average was computed using a centered window of length L, so that each value represents the mean of observations symmetrically distributed around the point in time. This ensures that the smoothed series remains aligned in phase with the original signal, avoiding the temporal shifts that occur when the averaging is performed only over past values. At the boundaries of the time series, the first and last $L/2$ data points are discarded to ensure a consistent reconstruction of the low-frequency signal modulated by GCRs.

The window length L was optimized in terms of attenuation of high-frequency atmospheric variability and transmission of the 11-year modulation. A trade-off study was conducted by defining the attenuation $A(T;L)$ through the amplitude response of the L-point moving-average filter, $H(T;L)$ [39], which can be expressed as:

$$|H(T;L)| = \frac{|\sin(\pi L/T)|}{L\,|\sin(\pi/T)|}\,. \tag{3}$$

where T denotes the oscillation period (in months) of the component under investigation. The attenuation can be then expressed as:

$$A(T;L) = 1 - |H(T;L)|\,. \tag{4}$$

In the present work, the detrending method was applied exclusively to the ^{7}Be time series: the neutron counts and sunspot number series were analyzed in their original form, as they are considered physical drivers of ^{7}Be concentration and already represent temporally smoothed indices of cosmic ray flux and solar activity, respectively. This approach avoids the introduction of mathematical artifacts and preserves the physical meaning of the time series.

2.4. Correlation Metrics and Confidence Intervals Evaluation

The investigation of correlations among variables characterized by (quasi-)sinusoidal periodicity, phase shifts, and inherent temporal lags, such as the detrended time series of atmospheric ^{7}Be concentrations, sunspot numbers, and ground-level neutron fluxes, requires careful methodological considerations. The present work aims to investigate the linear correlation between the monthly ^{7}Be time series and cosmic drivers. For this reason Pearson's correlation coefficient is evaluated as the primary correlation metric on the detrended beryllium time series and cosmic drivers. In addition to Pearson's r, the rank-based coefficients Spearman's ρ and Kendall's τ are reported as secondary correlation metrics which capture monotonic association irrespective of functional form. Their consistency with r is evaluated according to three criteria: (i) ρ and τ share the sign of r; (ii) their 95% confidence intervals (CIs) exclude zero; (iii) the estimates are stable under reasonable analysis choices (e.g., smoothing window, sample period, or moderate lags). Pronounced deviations between r and the rank-based measures are interpreted as signals of nonlinearity, influential episodes, or violation of the model assumptions. For the following discussion, it has assumed that the two time series, whose correlation is to be investigated, can be expressed as vectors of observations:

$$X = (x_1, x_2, \ldots, x_i, \ldots, x_n) \quad \text{and} \quad Y = (y_1, y_2, \ldots, y_j, \ldots, y_n). \tag{5}$$

where n denotes the number of observations, and x_i and y_j represent the values of the variables X and Y at time indices i and j, respectively. These generic representations will be used consistently throughout the following discussion.

2.4.1. Correlation Metrics

The correlation metrics used in this work, are briefly introduced below:

- Pearson's correlation coefficient r—the metric measures the strength and direction of a linear relationship between two variables. According to [38], it is defined as:

$$r = \frac{\mathrm{Cov}(X, Y)}{\sigma_X \, \sigma_Y} \tag{6}$$

  where $\mathrm{Cov}(X, Y)$ denotes the covariance between X and Y, and σ_X and σ_Y are the standard deviations of X and Y, respectively.
- Spearman's rank correlation coefficient ρ [40]—the metric measures the strength and direction of a monotonic relationship by computing the Pearson correlation between the ranked values of the variables:

$$\rho = \frac{\mathrm{Cov}(\mathrm{rank}(X), \mathrm{rank}(Y))}{\sigma_{\mathrm{rank}(X)} \, \sigma_{\mathrm{rank}(Y)}} \tag{7}$$

  where Cov and σ have the same meaning as in the Pearson case, but are applied to the ranked variables. Spearman's ρ is particularly effective in detecting relationships that are nonlinear but still consistently increasing or decreasing.
- Kendall's rank correlation coefficient τ [41,42]—the metric is based on counting the number of concordant and discordant pairs among all possible pairs of observations:

$$\tau = \frac{n_c - n_d}{\frac{1}{2} n(n-1)} \tag{8}$$

  where n_c and n_d are the numbers of concordant and discordant pairs of observations respectively, and n represents the sample size. Two observations are concordant if the ordering of their ranks for both variables is consistent, and discordant otherwise.

While all three measures capture associations between variables, they differ in their sensitivity and interpretation. Pearson's r assesses the strength and direction of a linear relationship and assumes normally distributed data. In contrast, Spearman's ρ and Kendall's τ are rank-based measures that capture monotonic relationships without requiring linearity. Kendall's τ tends to be more reliable for small sample sizes and provides a probabilistic interpretation, representing the difference between the probability that pairs of observations are in the same order versus different orders. Spearman's ρ can be slightly more sensitive to variations in the strength of monotonic associations but may be more influenced by extreme values in the ranks. Together, these correlation coefficients offer complementary insights into both linear and nonlinear associations in the data.

2.4.2. Confidence Intervals Evaluation

Estimating uncertainty for correlation coefficients in long monthly records raises two methodological concerns. First, with large sample sizes n, classical significance tests tend to yield vanishing p-values even for trivially small effects, offering little information about effect magnitude. Second, monthly geophysical series typically retain serial correlation, which can even be increased by smoothing procedures such as running averages. For this reason, confidence intervals computed under the assumption of independence among observations may be underestimated. In this work, the presence of autocorrelation is explicitly accounted for by constructing CIs with the moving–block bootstrap (MBB) procedure [43,44]. In this approach, the original time series is partitioned into consecutive blocks of length b, where each block overlaps with the next one by $b-1$ observations. Bootstrap replicates are then generated by randomly sampling these blocks with replacement and concatenating them until a series of the original length is reconstructed. In this way, the bootstrap replicates preserve the short-term autocorrelation up to $b-1$ consecutive observations in the structure of the data.

In our implementation, resampling is performed jointly on contemporaneous pairs of observations $Z_t = (X_t, Y_t)$ (detrended ^{7}Be and the driver), with $B = 2000$ bootstrap replicates. For each replicate, the correlation metric of interest (Pearson's r, Spearman's ρ, Kendall's τ) is recomputed, yielding an empirical sampling distribution that directly provides percentile $(1-\alpha)$ confidence intervals accounting for serial correlation. The block length b is selected adaptively by computing the Ordinary Least Squares (OLS) [38,45] residuals between the original and the smoothed ^{7}Be time series. The integrated autocorrelation time (IACT) [37,46] is then applied to the residuals, so that it captures the persistence of the unexplained variance autocorrelation. The block length b is finally set to the minimum value that preserves this dependence. A stability study is also performed by varying the block length within a reasonable range, in order to evaluate how the confidence intervals depend on b values.

3. Results

3.1. Correlation on the Raw Data

The correlation between ^{7}Be, neutron flux, and sunspot number were initially evaluated using raw, non-detrended data. This preliminary analysis was conducted to establish a baseline reference for comparison with the results obtained after applying detrending technique.

In the left (a) and in the middle (b) panels of Figure 2 are shown scatter plots between ^{7}Be concentration and neutron flux, and between ^{7}Be and sunspot number, both of which show cloud-like point distributions where a linear association is not immediately evident. In contrast, the right panel (c) reveals a clear negative linear trend between neutron flux and sunspot number, reflecting the common solar modulation signal. This strong

interdependence supports the use of both neutron counts and sunspot number as external drivers of ^{7}Be variability, even without detrending.

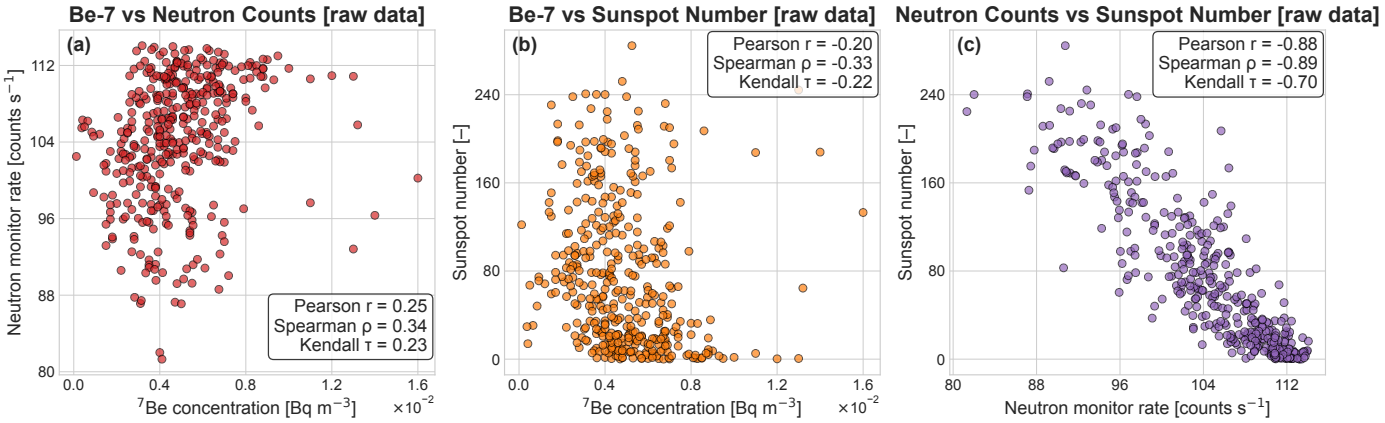

Figure 2. Scatter plots showing the relationships among the investigated variables using raw monthly data. Pearson, Spearman and Kendall metrics values are reported in the legends.

Correlation metrics index and related confidence intervals are summarized in Table 1.

Table 1. Correlation coefficients computed for the analyzed variable pairs on raw variables (moving-block bootstrap: $b = 8$, $B = 2000$).

Pair	r	95% CI (r)	ρ	95% CI (ρ)	τ	95% CI (τ)
Be-7 vs. Neutron Count	0.25	[0.11, 0.42]	0.34	[0.20, 0.51]	0.23	[0.14, 0.34]
Be-7 vs. Sunspot Number	−0.20	[−0.38, −0.03]	−0.33	[−0.50, −0.17]	−0.22	[−0.34, −0.11]
Neutron Count vs. Sunspot Number	−0.88	[−0.92, −0.81]	−0.89	[−0.92, −0.81]	−0.70	[−0.75, −0.61]

For the analysis on raw data, the block length was set to b = 8, in line with the adaptive estimate from the IACT of OLS residuals (see Section 2.4.2). The analysis of raw data indicates that the relationship between atmospheric ^{7}Be concentration and both solar and cosmic proxies is modest, with correlation coefficients around 0.2–0.3 in absolute value. Although the confidence intervals exclude zero, confirming that the associations are statistically significant, their magnitude remains much smaller than that observed for the neutron counts–sunspot pair. This suggests that ^{7}Be does not respond to solar and cosmic drivers as directly as neutron monitors, but rather integrates additional atmospheric processes that may obscure or modulate the primary signal. These findings highlight the necessity to isolate the intrinsic, large-scale modulation of ^{7}Be induced by solar and cosmic factors, which may otherwise be masked by dominant seasonal patterns and atmospheric variability.

3.2. Running Average Results

Window length L optimization was carried out by calculating the attenuation $A(T; L)$ of the various contributions for values of L ranging from 24 to 70 months. Results are summarized in Figure 3. With $L = 48$ months the variability around 11 years is largely preserved (mean attenuation ≈ 20%, i.e., ≈80% transmission), while fluctuations on shorter time scales are strongly suppressed (mean attenuation ≈ 80%), thus providing a clear separation of time scales without excessively damping the 11-year signal.

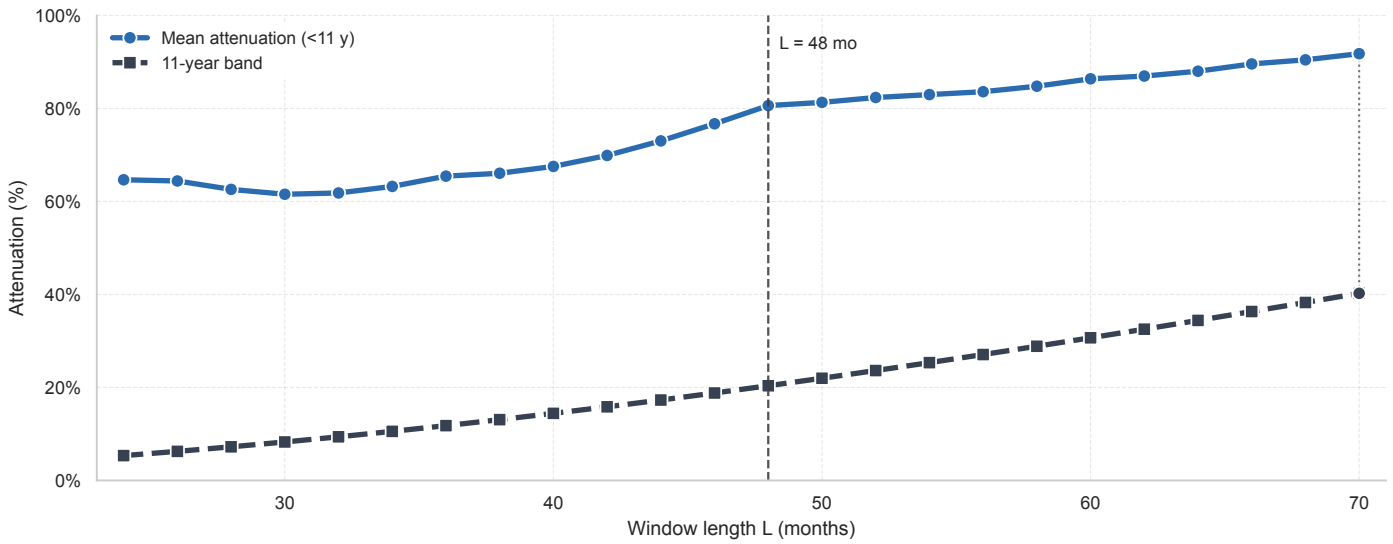

Figure 3. Attenuation $A(T;L)$ for atmospheric and cosmic and solar contributions for different window length L. The blue curve (color online) reports the mean attenuation of variability with periods shorter than 11 years (atmospheric), while the grey curve shows the attenuation of the 11-year contribution (cosmic and solar).

The smoothed ^{7}Be time series with a $L = 48$-month window is shown in Figure 4. For the ^{7}Be smoothed series, the effective number of independent observations, evaluated accordingly to [47], is $N_{\text{eff}} \approx 12.9$, i.e., 3.2% of the nominal $N_{\text{core}} = 397$ observations. This reduction of information is explicitly accounted for when constructing 95% confidence intervals via a moving–block bootstrap.

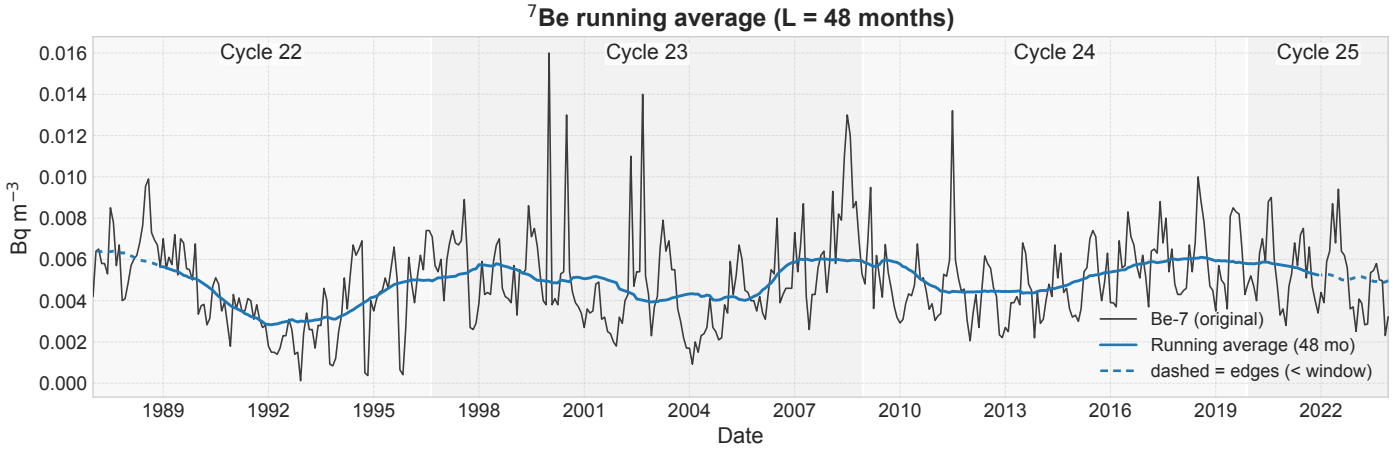

Figure 4. Running average results for the monthly concentrations of ^{7}Be measured at Casaccia site (black). Blue line (color online) shows the low-frequency trends extracted using the running average with a 48-month window. Shaded background bands represent Solar Cycles 22 to 25.

Using peak-to-peak spacing as a descriptive metric, varying the window by ±15 months, a period of $T = 10.0 \pm 0.1$ years is obtained for ^{7}Be concentration. The shortening of this period compared to the 11 years modulation, should be interpreted as the effect of time-varying phase lags and beating with seasonal/QBO/ENSO variability. These mechanisms can shift local maxima and minima and can produce an apparent shortening of the cycle, without altering the fundamental frequency determined by the heliospheric-modulated cosmic driver.

3.3. Correlation Metrics Results

The correlation among the investigated time series were assessed using the metrics described in Section 2.4. Pearson's correlation coefficient, together with its confidence interval, represents the primary metric of this study. Results obtained with a running-mean window of $L = 48$ months and a block length of $b = 36$ months are shown in Figure 5. The rank-based coefficients ρ (Spearman) and τ (Kendall), together with their confidence intervals, are reported as consistency checks, confirming the correlation pattern identified by Pearson's coefficient.

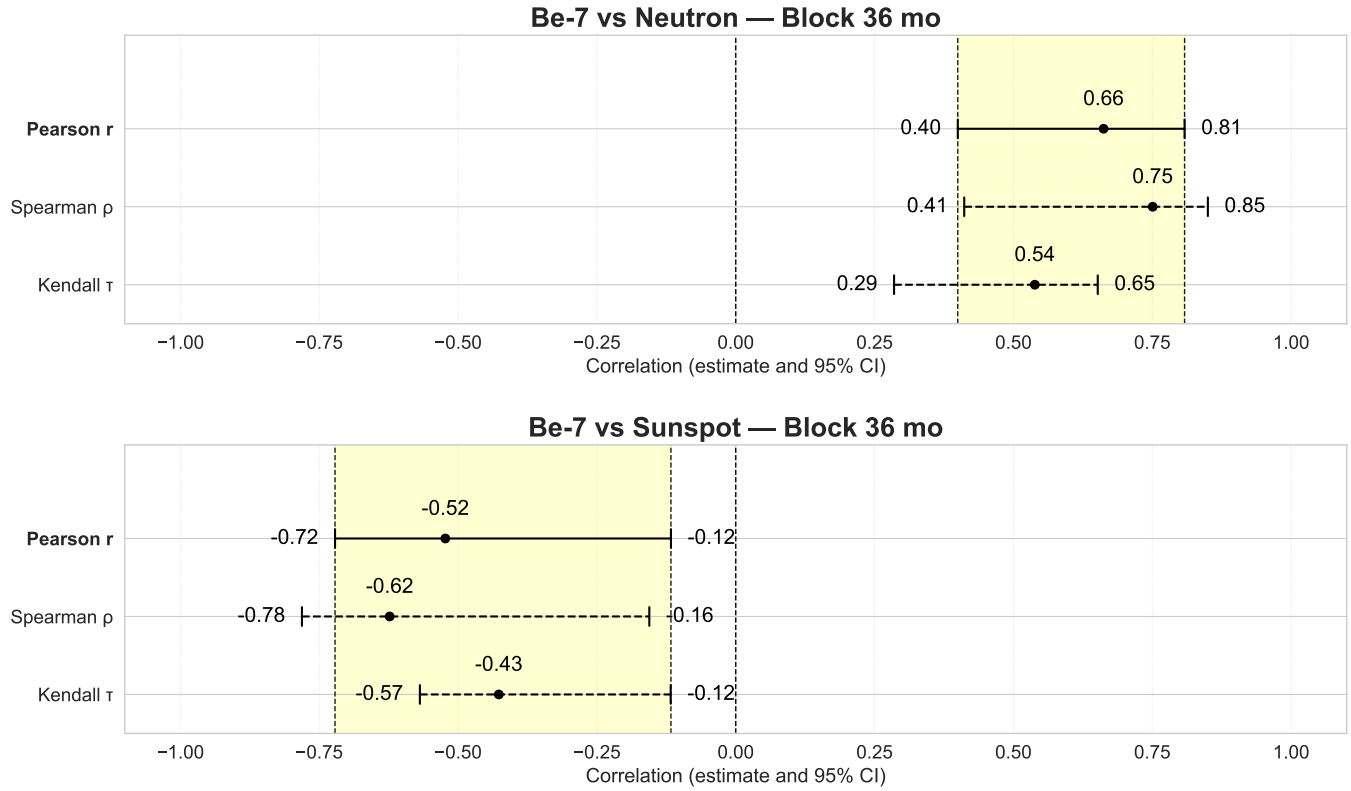

Figure 5. Correlation estimates between monthly ^{7}Be concentrations (low-pass filtered with a 48-month running average) and two solar–cosmic drivers: ground-level neutron counts (top) and sunspot numbers (bottom). Dots indicate the point estimates for Pearson's r, Spearman's ρ, and Kendall's τ; horizontal bars represent the 95% confidence intervals obtained with the moving block bootstrap (block length $b = 36$ months). The shaded yellow area (color online) highlights the Pearson's r confidence interval.

3.3.1. Sensitivity to the Smoothing Window Length

The stability of correlation estimates was assessed by varying the length of the centered running average used as low-pass filter. Correlation coefficients (Pearson, Spearman, and Kendall), together with their confidence intervals, were computed for smoothing windows ranging from 24 to 60 months. Results are summarized in Table 2, where $L = 48$ months is explicitly marked as the reference choice.

Table 2. Correlation coefficients estimated with different smoothing windows L lengths (block $b = 36$). The column at $L = 48$ is set as reference.

Metric	$L = 48$	$L = 24$	$L = 36$	$L = 60$
Be-7 vs. Neutron				
Pearson r	**0.66**	**0.53**	**0.62**	**0.69**
Spearman ρ	0.75	0.62	0.73	0.77
Kendall τ	0.54	0.43	0.51	0.57
Be-7 vs. Sunspot				
Pearson r	**−0.52**	**−0.41**	**−0.48**	**−0.52**
Spearman ρ	−0.62	−0.53	−0.61	−0.62
Kendall τ	−0.44	−0.37	−0.41	−0.44

The results indicate that correlation estimates are relatively stable in the considered window range, with all estimates being consistent within their confidence intervals (Figure 6). Similar results are obtained with the rank-based metrics ρ and τ.

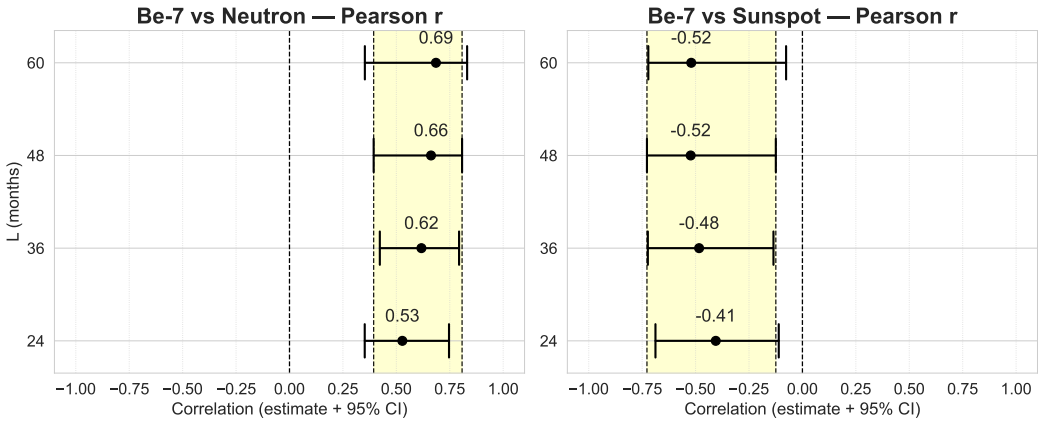

Figure 6. Correlation estimates between monthly ^{7}Be concentrations and the two cosmic drivers for different low-pass windows L (24–60 months): neutron counts (**left**) and sunspot numbers (**right**). Dots indicate Pearson's r coefficient values, with horizontal bars representing the 95% confidence intervals obtained via block bootstrap (block length $b = 36$ months). The shaded yellow area highlights the confidence interval for the reference window of $L = 48$ months.

3.3.2. Sensitivity of Confidence Intervals to Block Length b

Beyond the smoothing window L, the stability of the results was further assessed by analyzing the sensitivity of the confidence–interval (CI) estimates to the block length b employed in the moving–block bootstrap. Table 3 reports, for each correlation metric, the CI bounds obtained with the reference configuration ($b = 36$), together with the values for shorter ($b = 24$) and longer ($b = 48$) blocks. In addition to the lower and upper limits, the relative variation in CI width with respect to the reference case is also provided.

Table 3. Confidence-interval edges for correlation metrics at the reference block length ($b = 36$) and percentage change in CI width for alternative blocks ($b = 24, 48$). Width = high−low; Δwidth% is relative to $b = 36$.

Metric	BL = 36 (Ref)			BL = 24			BL = 48		
	Low	High	Width	Low	High	ΔWidth%	Low	High	ΔWidth%
Be-7 vs. Neutron									
Pearson *r*	**0.40**	**0.81**	**0.41**	**0.44**	**0.83**	−4.5	**0.37**	**0.81**	+8.6
Spearman ρ	0.41	0.85	0.44	0.41	0.86	+2.4	0.38	0.85	+6.6
Kendall τ	0.29	0.65	0.37	0.32	0.65	−10.0	0.27	0.65	+2.0
Be-7 vs. Sunspot									
Pearson *r*	**−0.72**	**−0.12**	**0.60**	**−0.74**	**−0.17**	**−5.7**	**−0.72**	**−0.09**	**+4.0**
Spearman ρ	−0.78	−0.16	0.63	−0.79	−0.20	−5.3	−0.78	−0.12	+4.3
Kendall τ	−0.57	−0.12	0.45	−0.58	-0.16	−8.2	−0.57	−0.09	+5.7

4. Discussion

The analysis of the raw time series data (see Table 1), performed to establish reference values in the present study, reveals weak correlation between the atmospheric ^{7}Be concentration and both neutron counts, a proxy variable for the cosmic ray flux reaching Earth, and the sunspot number, a proxy for solar activity. Despite its small magnitude, Pearson's coefficient is positive with a 95% CI entirely above zero for ^{7}Be vs neutron counts, and negative with a 95% CI entirely below zero for ^{7}Be vs sunspot number. This pattern is consistent with the underlying physics: atmospheric ^{7}Be is produced by spallation of N and O nuclei by galactic cosmic rays, for which neutron monitors provide a near-proxy for the secondary hadronic cascade at ground level. By contrast, solar activity affects ^{7}Be only indirectly via heliospheric modulation of the galactic cosmic-ray flux. Consequently, the observed correlation is weaker and its uncertainty larger, which is the expected outcome of the indirect coupling. The rank-based coefficients ρ and τ were included as consistency checks and show the same sign as Pearson's coefficient: their 95% CIs lie entirely above zero for ^{7}Be–neutron and entirely below zero for ^{7}Be–sunspot. As a benchmark, neutron counts and sunspot number exhibit the expected strong anti-correlation, with tight confidence intervals well separated from zero. These findings support the conservative hypothesis adopted in this work to avoid detrending the neutron count and sunspot number time series, as they already capture almost all the information regarding the two cosmic phenomena of interest. A centered running average was used in this work as a linear, zero-phase low-pass filter to suppress atmospheric dynamics contribution to the signal. The window length L was selected considering a trade-off in terms of attenuation $A(L;T)$ of the different contributions (Figure 3): L should maximize the attenuation of high-frequency components (periods shorter than 11 years) while minimizing the loss of the low-frequency signal, in particular the 11-year band (132 months). In this work a window of $L = 48$ months was selected, to reduce the < 11 y variability by about 80% preserving the larger part of the 11-year component, which is attenuated by only 20%. This detrending is necessary to isolate the co-variability with cosmic-ray drivers; without it, shorter-term atmospheric variability partly masks the correlation. At the same time, the running average, being a low-pass filter, increases serial dependence among successive observations, which reduces the effective degrees of freedom and consequently widens the confidence intervals at a given confidence level. Accordingly, uncertainty estimates should be obtained with methods that explicitly account for serial dependence rather than assuming independent observations, such as the moving–block bootstrap (MBB) adopted in this work. This method resamples contiguous blocks of the bivariate series to appropriately account for short-range serial dependence in the filtered monthly data, yielding uncertainty estimates that do not rely on independence assumptions. Presented results about the Pearson's coefficient for L = 48 and b = 36 months

indicate a positive correlation between atmospheric ^{7}Be and neutron counts ($r \approx 0.66$; 95% CI $[0.40, 0.81]$) and a negative correlation with the sunspot number ($r \approx -0.52$; 95% CI $[-0.72, -0.12]$). Confidence intervals, which exclude zero value, confirm the signs of the correlations at 95% C.L. Spearman's ρ and Kendall's τ exhibit the same sign as Pearson's r, their confidence intervals at the 95% level do not overlap zero, and the values remain stable across alternative smoothing windows. This convergence of metrics indicates that the correlations are statistically consistent, while the absence of pronounced discrepancies between r and the rank-based measures suggests that nonlinear effects or influential episodes do not dominate the observed associations.

5. Conclusions

In this study, the correlation between stratospheric ^{7}Be concentrations, measured at the ENEA Casaccia site from 1987 to 2024, and proxies of cosmic ray flux and solar activity was investigated. The application of a running average as low-pass filter to the atmospheric ^{7}Be time series allows the extraction of the low-frequency component influenced by the cosmic drivers. The Pearson coefficient evaluated for ^{7}Be and neutron counts (proxy of GCR) is positive and statistically significant, as confirmed by moving–block bootstrap confidence intervals, while a negative association is found with the sunspot number. These findings are consistent with the role of GCR flux as the direct driver of atmospheric ^{7}Be production via spallation in the stratosphere, and with the modulation exerted by solar activity through its impact on cosmic ray intensities. These results highlight the predominantly linear associations between ^{7}Be and cosmic phenomena, although the presence of nonlinear contributions cannot be excluded. The evidence, evaluated within a statistically consistent framework, supports an $\sim$11-year correlation between ^{7}Be and cosmic drivers. Consequently, atmospheric ^{7}Be can be regarded as a reliable tracer of cosmic ray variability and, indirectly, of solar modulation. Given the extensive global network of atmospheric ^{7}Be monitoring stations and the large datasets accumulated over decades, ^{7}Be records represent a promising resource for reconstructing past trends in galactic cosmic ray flux on Earth and may potentially contain valuable information related to solar activity variations.

While this work focuses on the decadal component of ^{7}Be and its link to cosmic and solar drivers, the same records enable investigation of seasonal/inter-annual variability due to atmospheric transport (e.g., Arctic Oscillation and related teleconnections). That analysis will be presented in a dedicated study.

Author Contributions: Conceptualization, A.R. and P.R.; methodology, A.R.; software, A.R.; validation, I.V., E.M.B., L.S.; formal analysis, A.R. and P.R.; resources, I.V.; data acquisition G.A., M.A., N.d.M., F.Z., G.l.N.; writing—original draft preparation, A.R. and L.C.; writing—review and editing, A.R. and L.C. All authors have read and agreed to the published version of the manuscript.

Funding: This research received no external funding.

Data Availability Statement: The ^{7}Be concentration data used in this study are available from the corresponding author upon reasonable request. The datasets related to cosmic ray flux (neutron counts) and solar activity (sunspot numbers) are publicly accessible through the open science repositories cited in the references.

Acknowledgments: The authors would like to thank all the ENEA colleagues who, over the years, have contributed to the collection of the ^{7}Be data used in this study. Their long-standing efforts provided the foundation for this work. The authors acknowledge the use of artificial intelligence (AI) tools to improve the English language style of the manuscript in the final phase of editing. Specifically, ChatGPT 4.5 (OpenAI, San Francisco, CA, USA) was employed as a writing aid for

grammar refinement and clarity, while the authors retained full responsibility for the scientific content, data analysis, and conclusions.

Conflicts of Interest: The authors declare no conflicts of interest.

Abbreviations

The following abbreviations and symbols are used in this manuscript:

CI	Confidence Interval
ENSO	El Niño–Southern Oscillation
GCR	Galactic Cosmic Rays
HPGe	High-Purity Germanium (detector)
IACT	Integrated Auto-Correlation Time
MDA	Minimum Detectable Activity
OLS	Ordinary Least Squares
QBO	Quasi-Biennial Oscillation
SEP	Solar Energetic Particles
r	Pearson's correlation coefficient
ρ	Spearman's rank correlation coefficient
τ	Kendall's rank correlation coefficient

References

1. Libby, W.F. Atmospheric Helium Three and Radiocarbon from Cosmic Radiation. *Phys. Rev.* **1946**, *69*, 671. [CrossRef]
2. Arnold, J.R.; Al-Salih, H.A. Beryllium-7 produced by cosmic rays. *Science* **1955**, *121*, 451–453. [CrossRef]
3. Young, J.A.; Silker, W.B. Aerosol deposition velocities on the Pacific and Atlantic Oceans calculated from ^{7}Be measurements. *Earth Planet. Sci. Lett.* **1980**, *50*, 92–104. [CrossRef]
4. Sanak, J.; Lambert, G.; Ardouin, B. Measurement of stratosphere-to-troposphere exchange in Antarctica by using short-lived cosmonuclides. *Tellus B* **1985**, *37*, 109–115. [CrossRef]
5. Mohan, M.P.; D'Souza, R.S.; Nayak, S.R.; Kamath, S.S.; Shetty, T.; Kumara, K.S.; Mayya, Y.S.; Karunakara, N. Influence of rainfall on atmospheric deposition fluxes of ^{7}Be and ^{210}Pb in Mangaluru (Mangalore) at the Southwest Coast of India. *Atmos. Environ.* **2019**, *202*, 281–295. [CrossRef]
6. Liu, H.; Considine, D.B.; Horowitz, L.W.; Crawford, J.H.; Rodriguez, J.M.; Strahan, S.E.; Damon, M.R.; Steenrod, S.D.; Xu, X.; Kouatchou, J.; et al. Using beryllium-7 to assess cross-tropopause transport in global models. *Atmos. Chem. Phys.* **2016**, *16*, 4641–4659. [CrossRef]
7. Liu, J.; Starovoitova, V.N.; Wells, D.P. Long-term variations in the surface air ^{7}Be concentration and climatic changes. *J. Environ. Radioact.* **2013**, *116*, 42–47. [CrossRef] [PubMed]
8. Schaar, K.; Spiegl, T.; Sato, T.; Langematz, U. The impact of ENSO on near-surface Beryllium-7. *J. Environ. Radioact.* **2025**, *282*, 107592 . [CrossRef]
9. Papastefanou, C.; Ioannidou, A.; Stoulos, S.; Manolopoulou, M. Atmospheric deposition of cosmogenic ^{7}Be and ^{137}Cs from fallout of the Chernobyl accident. *Sci. Total Environ.* **1995**, *170*, 151–156. [CrossRef]
10. Todorović, D.; Popović, D.; Đurić, G. Concentration measurements of ^{7}Be and ^{137}Cs in ground level air in the Belgrade city area. *Environ. Int.* **1999**, *25*, 59–66. [CrossRef]
11. Phillips, G.W.; King, S.E.; August, R.A.; Ritter, J.C.; Cutchin, J.H.; Haskins, P.S.; McKisson, J.E.; Ely, D.W.; Weisenberger, A.G.; Piercey, R.B.; et al. Discovery of Be-7 Accretion in Low Earth Orbit. In Proceedings of the 14th Annual AAS Guidance and Control Conference, Keystone, CO, USA, 2–6 February 1991; DTIC Report AD-A236 614. Available online: https://apps.dtic.mil/sti/pdfs/ADA236614.pdf (accessed on 25 August 2025).
12. Mewaldt, R.A.; Stone, E.C.; Tylka, A.J. Enhanced beryllium-7 concentrations in the upper atmosphere following solar proton events. *Geophys. Res. Lett.* **2001**, *28*, 2585–2588. [CrossRef]
13. Chen, D.L.; Zell, S.E.; Paulikas, G.A. Observations of cosmogenic beryllium-7 in the mesosphere and lower thermosphere. *J. Atmos. Sol.-Terr. Phys.* **1993**, *55*, 707–714.
14. Golubenko, K.; Rozanov, E.; Kovaltsov, G.; Leppänen, A.-P.; Sukhodolov, T.; Usoskin, I. Chemistry-climate model SOCOL-AERv2-BEv1 with the cosmogenic Beryllium-7 isotope cycle. *Geosci. Model Dev. Discuss.* **2021**, *14*, 7605–7620 . [CrossRef]
15. Nelson, G.A. Space Radiation and Human Exposures, A Primer. *Radiat. Res.* **2016**, *185*, 349–358. [CrossRef] [PubMed]

16. Rizzo, A.; Borra, E.M.; Ciciani, L.; Di Fino, L.; Romoli, G.; Santi Amantini, G.; Sperandio, L.; Vilardi, I.; Narici, L. Foundations of radiological protection in space: The integrated multidisciplinary approach for next manned missions in deep space. *Eur. Phys. J. Plus* **2023**, *138*, 1001. [CrossRef]
17. Papastefanou, C.; Ioannidou, A. Beryllium-7 and solar activity. *Appl. Radiat. Isot.* **2004**, *61*, 1493–1495. [CrossRef] [PubMed]
18. Rajacic, M.M.; Todorovic, D.J.; Krneta Nikolic, J.D.; Puzovic, J.M. The impact of the Solar magnetic field on ^{7}Be activity concentration in aerosols. *Appl. Radiat. Isot.* **2017**, *125*, 27–29. [CrossRef]
19. Aldahan, A.; Hedfors, J.; Possnert, G.; Kulan, A.; Berggren, A.-M.; Söderström, C. Atmospheric impact on beryllium isotopes as solar activity proxy. *Geophys. Res. Lett.* **2008**, *35*, L21812. [CrossRef]
20. Kremenchutskii, D.A.; Konovalov, S.K. Beryllium-7 and its variability in the near-surface atmosphere of Crimea, the Black Sea region. *Atmos. Pollut. Res.* **2022**, *13*, 101406. [CrossRef]
21. Brattich, E.; Liu, H.; Tositti, L.; Considine, D.B.; Crawford, J.H. Processes controlling the seasonal variations in ^{210}Pb and ^{7}Be at the Mt. Cimone WMO-GAW global station, Italy: A model analysis. *Atmos. Chem. Phys.* **2017**, *17*, 1061–1080. [CrossRef]
22. Kulan, A.; Aldahan, A.; Possnert, G.; Vintersved, I. Distribution of ^{7}Be in surface air of Europe. *Atmos. Environ.* **2006**, *40*, 3855–3868. [CrossRef]
23. Baldwin, M.P.; Gray, L.J.; Dunkerton, T.J.; Hamilton, K.; Haynes, P.H.; Randel, W.J.; Holton, J.R.; Alexander, M.J.; Hirota, I.; Horinouchi, T.; et al. The quasi-biennial oscillation. *Rev. Geophys.* **2001**, *39*, 179–229. [CrossRef]
24. Casselman, J.W.; Lübbecke, J.F.; Bayr, T.; Huo, W.; Wahl, S.; Domeisen, D.I.V. The teleconnection of extreme El Niño–Southern Oscillation (ENSO) events to the tropical North Atlantic in coupled climate models. *Weather Clim. Dyn.* **2023**, *4*, 471–487. [CrossRef]
25. Yu, N.; Chen, G.; Ray, J.; Chen, W.; Chao, N. Semi-decadal and decadal signals in atmospheric excitation of length-of-day. *Earth Space Sci.* **2019**, *6*, 1205–1216. [CrossRef]
26. Lal, D.; Peters, B. Cosmic Ray Produced Radioactivity on the Earth. In *Kosmische Strahlung II/Cosmic Rays II*; Sitte, K., Ed.; Handbuch der Physik/Encyclopedia of Physics; Springer: Berlin/Heidelberg, Germany, 1967; Volume 9, pp. 551–612, ISBN 3540038558.
27. Talpos, S.; Cuculeanu, V. A Study of the Vertical Diffusion of ^{7}Be in the Atmosphere. *J. Environ. Radioact.* **1997**, *36*, 93–106. [CrossRef]
28. Sitte, K.; Stierwalt, D.L.; Kofsky, I.L. Development of Air Showers in the Atmosphere. *Phys. Rev.* **1954**, *94*, 988–993. [CrossRef]
29. Papastefanou, C.; Ioannidou, A. Beryllium-7 Aerosols in Ambient Air. *Environ. Int.* **1996**, *22*, S125–S130. [CrossRef]
30. Zheng, M.; Liu, H.; Adolphi, F.; Muscheler, R.; Lu, Z.; Wu, M.; Prisle, N.L. Simulations of ^{7}Be and ^{10}Be with the GEOS-Chem global model v14.0.2 using state-of-the-art production rates. *Geosci. Model Dev.* **2023**, *16*, 7037–7057. [CrossRef]
31. Zhang, F.; Wang, J.; Baskaran, M.; Zhong, Q.; Wang, Y.; Paatero, J.; Du, J. A global dataset of atmospheric ^{7}Be and ^{210}Pb measurements: Annual air concentration and depositional flux. *Earth Syst. Sci. Data* **2021**, *13*, 2963–2994. [CrossRef]
32. Yoshimori, M. Beryllium 7 radionuclide as a tracer of vertical air mass transport in the troposphere. *Adv. Space Res.* **2005**, *36*, 828–832. [CrossRef]
33. Koch, D.M.; Jacob, D.J.; Graustein, W.C. Vertical transport of tropospheric aerosols as indicated by ^{7}Be and ^{210}Pb in a chemical tracer model. *J. Geophys. Res. Atmos.* **1996**, *101*, 18651–18666. [CrossRef]
34. Długosz-Lisiecka, M.; Bem, H. Seasonal fluctuation of activity size distribution of ^{7}Be, ^{210}Pb, and ^{210}Po radionuclides in urban aerosols. *J. Aerosol Sci.* **2020**, *144*, 105544. [CrossRef]
35. NMDB Event Search Tool (NEST). Available online: https://www.nmdb.eu/nest/ (accessed on 25 October 2024).
36. WDC-SILSO. Royal Observatory of Belgium, Brussels. Available online: https://www.sidc.be/SILSO/datafiles (accessed on 25 October 2024).
37. von Storch, H.; Zwiers, F.W. *Statistical Analysis in Climate Research*; Cambridge University Press: Cambridge, UK, 1999; ISBN 0521450713/0521012309.
38. Wilks, D.S. *Statistical Methods in the Atmospheric Sciences*, 3rd ed.; International Geophysics Series; Academic Press: San Diego, CA, USA, 2011; Volume 100, ISBN 978-0123850225.
39. Oppenheim, A.V.; Schafer, R.W. *Discrete-Time Signal Processing*, 3rd ed.; Pearson: Upper Saddle River, NJ, USA, 2010; p. 47, ISBN 978-0131988422.
40. Spearman, C. The Proof and Measurement of Association Between Two Things. *Am. J. Psychol.* **1904**, *15*, 72–101. [CrossRef]
41. Kendall, M.G. A New Measure of Rank Correlation. *Biometrika* **1938**, *30*, 81–93. [CrossRef]
42. Conover, W.J. *Practical Nonparametric Statistics*, 3rd ed.; John Wiley & Sons: New York, NY, USA, 1999; ISBN 978-0471160687.
43. Künsch, H.R. The jackknife and the bootstrap for general stationary observations. *Ann. Statist.* **1989**, *17*, 1217–1241. [CrossRef]
44. Lahiri, S.N. *Resampling Methods for Dependent Data*; Springer Series in Statistics; Springer: New York, NY, USA, 2003; ISBN 978-0387954417.
45. Seber, G.A.F.; Lee, A.J. *Linear Regression Analysis*, 2nd ed.; Wiley Series in Probability and Statistics; Wiley-Interscience: Hoboken, NJ, USA, 2003; ISBN 978-0471415404.

46. Sokal, A.D. Monte Carlo methods in statistical mechanics: Foundations and new algorithms. In *Functional Integration: Basics and Applications*; DeWitt-Morette, C., Cartier, P., Folacci, A., Eds.; NATO ASI Series B: Physics; Springer: Boston, MA, USA, 1997; Volume 361, pp. 131–192. ISBN 978-0306456577. [CrossRef]
47. Bartlett, M.S. On the Theoretical Specification and Sampling Properties of Autocorrelated Time-Series. *J. R. Stat. Soc. Suppl.* **1946**, *8*, 27–41. [CrossRef]